CHAPTER 3 ION IMPLANTATION

When an energetic ion penetrates a material it loses energy until it comes to rest inside the material. The energy is lost via inelastic and elastic collisions with the target atoms. When an ion has lost all its energy and comes to rest in the substrate, it is said to be implanted in the material. Consequently this technique is known as ion implantation. It is widely used in the manufacturing of semiconductors' electronic devices and in different material doping processes. If this technique is used, it is important to be able to predict the final distribution of the ions in the material. This can only be achieved if all the processes involved until the ion comes to rest inside the material of interest are clearly understood. Hence this chapter describes the most important processes that occur during ion implantation.

3.1 STOPPING POWER

Energy loss by ions in a material is the factor which determines the final distribution of ions and defects. Since the ion loses its energy (E) per penetration depth (x), where x is the distance within the target measured from the surface of the target, the energy loss in a material, which is referred to as the stopping power or energy loss, is defined as dE/dx.

An energetic ion penetrating a material loses its energy mainly via two processes which are considered to be independent of each other. They are: nuclear energy loss and electronic energy loss. Therefore, the stopping can also be separated into nuclear stopping and electronic stopping. These are described in sections 3.1.1 and 3.1.2 respectively. From the two stopping powers the total stopping power (S) can be written as:

$$S = \frac{dE}{dx} = \left(\frac{dE}{dx}\right)_n + \left(\frac{dE}{dx}\right)_e \qquad \text{....3.1}$$

where the stopping powers with subscript n and e represent nuclear and electronic stopping power respectively.

From the total stopping power S, the stopping cross section can be calculated from dividing S by target density N':

$$\varepsilon = -\frac{dE}{N'dx} \qquad \ldots 3.2$$

The penetration length R of ions with initial incident energy of E_0 is given by:

$$R = \frac{1}{N'}\int_0^{E_0} \frac{dE}{dx} \qquad \ldots 3.3$$

The independence of nuclear stopping and electronic stopping suggests that the stopping power is strongly dependent on the energy E of the ion, as can be observed in figure 3-1below.

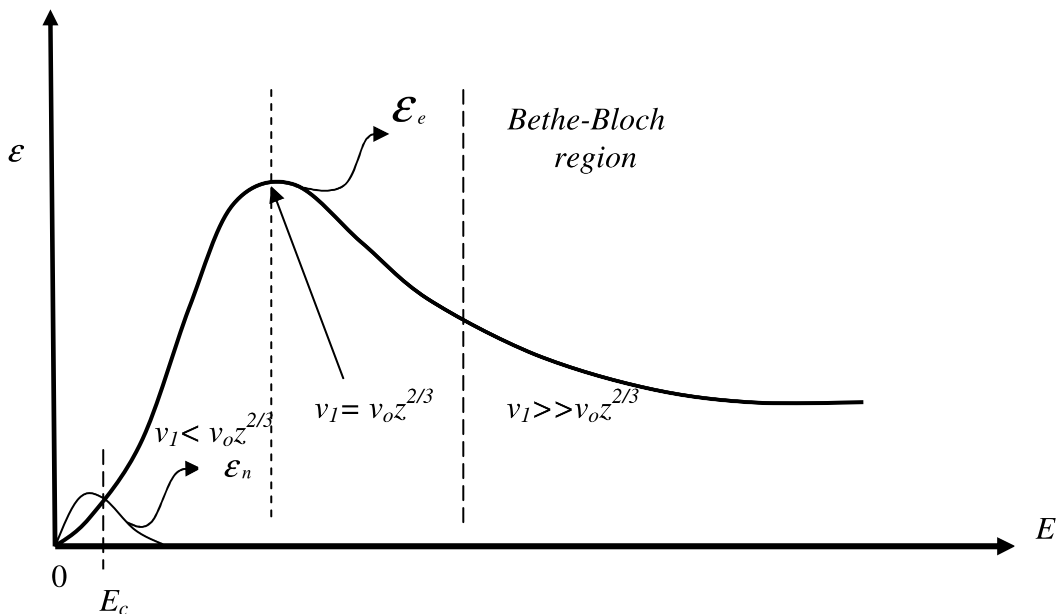

Figure 3-1: The dependences of electronic ε_e and nuclear ε_n contributions to the stopping cross section ε as a function of the ion energy E. The Bethe-Bloch equation [Bet30] is a good approximation at very high energies, v_1 is the velocity of an ion, v_o is the Bohr velocity and Z is the atomic number of the ion.

At low energies the nuclear stopping dominates while at high energy it decreases and electronic stopping dominates. Electronic stopping starts to dominate above the critical energy E_c (see figure 3-1), then reaches a maximum and decreases at the very high energy region or Bethe-Bloch region. This is caused by the shorter amount of time which the ion has to interact with the electrons of the target atoms owing to its high velocity. The details of figure 3-1 are discussed in subsections 3.1.1 and 3.1.2.

3.1.1 NUCLEAR STOPPING

Nuclear stopping power is the stopping process which includes all the processes that result in the transfer of energy from the implanted ion into the target atom as a whole. Therefore, the nuclear scattering can be described by the potential between an ion (1) and a target (2) atom. For example, in the head-on collisions case, where there is backscattering of the colliding ions from the target atoms due to repulsion between colliding ions and target nuclei, the interatomic potential between the two positive charges of ion and the target atoms can be written as:

$$V = \frac{Z_1 Z_2 e^2}{4\pi\varepsilon_0 r} \qquad \ldots 3.4$$

where Z_1 and Z_2 are the atomic numbers of ion and target respectively, e is the electron charge, ε_0 is the permittivity of free space and r is the interatomic distance. This potential is a pure Coulomb potential that does not take into account the screening effects. The scattered ions that result in a large scattering angle are said to be Rutherford backscattered. The analytical technique that is based on the analyses of the backscattered particles is discussed in chapter 4. From figure 3-1, it is evident that the probability of this Rutherford backscattering process is negligible for energetic ions since the nuclear stopping is dominant only at low energies.

There are many different methods of calculating interatomic potentials (which take screening effects into consideration): these are categorised into simple and complicated methods. The former are those that assume fixed charge distributions. In these methods different contributions to the interatomic potential are calculated independently as a function of interatomic distance r. The complicated methods are those that are performed directly from the first principles of quantum mechanics and require a large amount of numerical computations. The interatomic potentials for a wide number of atomic pairs have been calculated using the Hartree-Fock charge distributions method [Zie85] and have been found to be generally in agreement with the experimental data. From these results the analytical expression known as the universal interatomic potential was derived [Tes95]:

$$V_U = \frac{Z_1 Z_2 e^2}{4\pi\varepsilon_0 r} \Phi_U\left(\frac{r}{a_U}\right) \qquad \ldots 3.5$$

where the universal screening function $\Phi_U(x)$ and the screening radius $a_U(Z_1,Z_2)$ are given by fitted formulas [Zie85].

The energy transfer from the ion to the target atoms can be calculated using the interatomic potential between an ion and the target atom. Generally this is performed by taking into consideration the motion of all the N atoms in a system determined by N potentials. Such calculations are known as molecular dynamics (MD) simulations and are tedious but today they are used to study phenomena related to individual ion-target interactions. A simplification of this method has been developed, viz. the binary collision approximation (BCA), where collisions between two atoms at a time are considered. These methods break down at low energy when many body effects become important [Rim95].

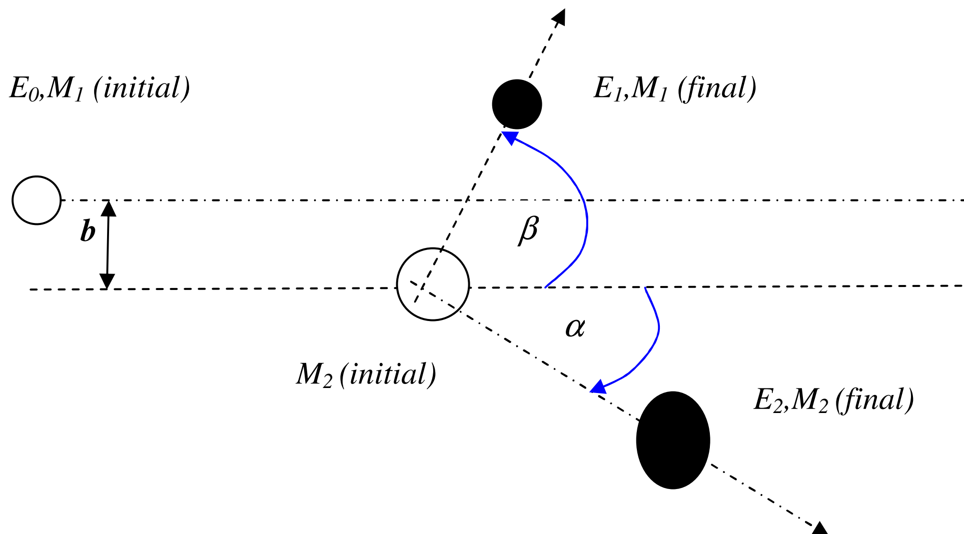

Figure 3-2: A schematic diagram showing the ion M_1 of initial energy E_0 colliding with the target atom M_2 (initial) causing it to move with E_2 and its own energy reducing to E_1.

The geometry of a collision between an energetic ion and a target atom is depicted in figure 3-2. In figure 3-2, an ion M_1 with an initial energy of E_0 is deflected by the target atom M_2. The position of M_2 relative to the M_1 trajectory is called the impact parameter and is represented by b (it is a projection of the projectile path to the target axis). During the collision M_1 and M_2 are deflected with angles relative to the M_1 original trajectory, α and β respectively. During the collision the kinetic energy T is

transferred from M_1 to M_2. From the conservation of energy and momentum the kinetic energy transfer can be calculated. When this is carried out, T is found to be a function of α, projectile energy E_0, the mass of the projectile M_1, and the mass of the target atoms M_2 in the laboratory system [Tho03]:

$$T = E_0 \frac{4M_1 M_2}{(M_1 + M_2)^2} \cos^2(\alpha) \qquad \ldots 3.6$$

and in the centre of the mass system:

$$T = E_0 \frac{4M_1 M_2}{(M_1 + M_2)^2} \sin^2(\frac{\alpha_c}{2}) \qquad \ldots 3.7$$

where α_c is the recoiling angle in the centre of this system.

The nuclear stopping is calculated from the integration over all the impact parameters:

$$\varepsilon_n = 2\pi \int_0^{b_{\max}} T(E, \alpha) b db \qquad \ldots 3.8$$

Using equation 3.5, a universal nuclear cross section can be determined as is done in [Zie85].

3.1.2 ELECTRONIC STOPPING

Electronic stopping is the process where an energetic ion penetrating a material loses its energy to the target electrons. The process of transferring the ion's kinetic energy to the target electrons is a complicated one compared to the nuclear stopping discussed in section 3.1.1, because it originates from different processes. Some of these are as follows: Direct kinetic energy transfers to electrons mainly due to electron-electron collisions, excitation or ionization of target atoms, excitation of conduction electrons, and excitation, ionization or electron-capture of the ion itself, etc. [Zie85a]. The complexity of these processes makes it difficult to describe the electronic energy loss in terms of one theory. Hence different models are applied for different ion energies to describe this process. The said energies are usually divided into three parts. These parts are separated by comparing the ion's velocity with the Bohr velocity $v_o = e^2/\hbar$, where e and $\hbar$ are the electron charge and Planck's constant

respectively. In this theory a hydrogen atom at 25 *keV* moves with the same velocity as its orbital electron, while helium moves with the same velocity as its orbital electrons at 252 *keV*. Hence, the ion's initial energy with velocity equal to orbital velocity can be written as a function of the ion's mass and atomic number as:

$$E = Z_1^{4/3} A_1 25 \quad keV \qquad \ldots 3.9$$

where Z_1 and A_1 are ion's atomic number and mass number respectively.

The first part is the low energy region. This is the part where the ion's velocity v_1 is less than $v_o Z^{2/3}$, i.e. $v_1 < v_o Z^{2/3}$. In this region the ion cannot transfer enough energy to the electrons that are much lower in energy than the Fermi level to excite them to unoccupied states. Therefore, in this region only electrons in the energy states close to the Fermi level contribute to energy loss. The electronic stopping for this region has been calculated by assuming a free electron gas with a density ρ that changes slightly with the location [Lin53][Lin61a][Lin61b]. In this model the electronic cross section of an ion with Z_1 can be written as [Zie85a]:

$$\varepsilon_e = \int I(v,\rho)(Z_1(v))^2 \rho dV \qquad \ldots 3.10$$

where ε_e is the electronic stopping cross section, I is the stopping interaction function of the particle (ion) of unit charge with velocity v, Z_1 is the charge of the particle, ρ is the electron density of the target and the integral is performed over each volume element dV of the target. If one considers the interaction with the charged particle to be a perturbation in the free electron gas (which is carried out by taking into account screening and polarization), then the state of the ion can be changed via charge transfers. Therefore, Z_1 in equation 3.10 can be replaced by an effective charge Z_1^*. The electron capture and electron loss depend greatly on the projectile velocity [Zie85b].

Since the transferred energy from the projectile to the target electron is proportional to the projectile velocity, the electronic stopping power is proportional to the projectile velocity as is given by [Lin53][Lin61a][Lin61b]:

$$\varepsilon_e = 19.2 \frac{Z_1^{7/6} Z_2 v_1}{(Z_1^{2/3} + Z_2^{2/3}) v_0} \quad \left[\frac{eVcm^2}{10^{15} at} \right] \qquad \ldots 3.11$$

where the Bohr velocity $v_0 = e^2/\hbar$.

The second part is the region where the ion velocity v_1 is far greater than $v_oZ^{2/3}$ i.e. $v_1 >> v_oZ^{2/3}$. In this region the ion is fully stripped of all its electrons. The energy loss is proportional to Z_1^2 as found by Bethe and Bloch. Hence this region is known as the Bethe-Bloch region, as indicated in figure 3-1. The electronic stopping in this region is given by the Bethe-Bloch equation [Boh13][Bet30] [Blo33][And77]:

$$\varepsilon_e = \frac{4\pi Z_1^2 Z_2 e^4}{m_e v_1^2}\left[\ln\left(\frac{2m_e v_1^2}{I}\right) + \ln\left(\frac{1}{1-\beta^2}\right) - \beta^2 - \frac{C}{Z_2}\right] \quad ...3.12$$

where m_e is the electron's mass, v_1 the velocity of the projectile, $\beta = v/c$ where c is the speed of light, I is the average ionisation potential and C/Z_2 is the shell correction. I is defined theoretically as $\ln I = \sum_n f_n \ln E_n$ and is very complicated except for simple target atoms. Here E_n and f_n are the possible energy transitions and corresponding oscillator strengths for target atoms. Hence the Thomas-Fermi model has been used to estimate I. The approximation is Bloch's rule: $I = Z_2 10\ eV$ [Blo33].

The third part is the intermediate one, i.e. between part 1 and part 2; i.e. the part where $v_1 \approx v_oZ^{2/3}$. In this case the ion is partly ionized and the electronic stopping reaches a maximum.

The important domains for the purposes of this thesis are the low and intermediate energy regions, since the study reports on the result of silver ions of 360 keV that were implanted into SiC (a low energy regime) and analysed by Rutherford backscattering spectroscopy (RBS) using 1.6 MeV α-particles (an intermediate energy regime).

3.2 ENERGY LOSS IN COMPOUNDS

The energy loss discussed to this point is that for a target consisting of one element. The energy loss in targets consisting of more than one element, i.e. the compounds, has not been discussed yet, but they are also the more common systems and are very

important in this study since we are working with SiC. Therefore, the purpose of this section is to discuss the energy loss in compounds.

If the target is a compound A_mB_n of two different elements A and B then the total stopping of an ion penetrating it can be found by using a simple additive rule. This rule is based on the assumption that the interaction processes between ions and component target are independent of the surrounding target atoms. Therefore, if the stopping cross sections of element A and B are written as ε^A and ε^B respectively, the total stopping cross section is:

$$\varepsilon^{A_mB_n} = m\varepsilon^A + n\varepsilon^B \qquad ...3.13$$

where m and n represent the relative molar fractions of the compound materials. Equation 3.13 is known as Bragg's rule [Bra05]. Experimentally the energy loss is found to slightly deviate from Bragg's rule owing to the chemical and physical state of the material. For example, deviations of the order of 10% - 20% from Bragg's rule are found in experimental results for the stopping maximum for light gases and solid compounds containing heavier elements [Zie85b][Zie88]. These deviations led to the development of a model with respect to correcting for the chemical state of the compound. This model is called the core and bonds model (CAB) [Zie88]. The CAB model estimates the compound's stopping power for compounds from the measured values of 114 organic compounds. In this model, each molecule is described as a set of atomic cores and bonds, corresponding to the non-bonding core and bonding valence electrons, respectively. Ziegler et al. [Zie88] has also used this model in calculating the stopping cross sections for some inorganic compounds. For this method to be successful, the bond structures of the compound must be known.

3.3 ENERGY STRAGGLING

An energetic ion penetrating a substrate loses its energy through many interactions with the target atoms, which result in interactions fluctuating statistically. This implies that identical ions with the same initial energy do not possess the same energy after penetrating a thickness Δx of the same medium. Hence, the energy loss ΔE is subjected to fluctuations. The ions having the energy loss ΔE caused by the stopping

powers of the material also spread to $\delta\Delta E$, which is due to statistical fluctuations in the nuclear energy loss and electronic energy loss. This discrete nature of the energy loss processes, resulting in uncertainty in energy or energy spread, is known as nuclear straggling and is depicted in figure 3-3.

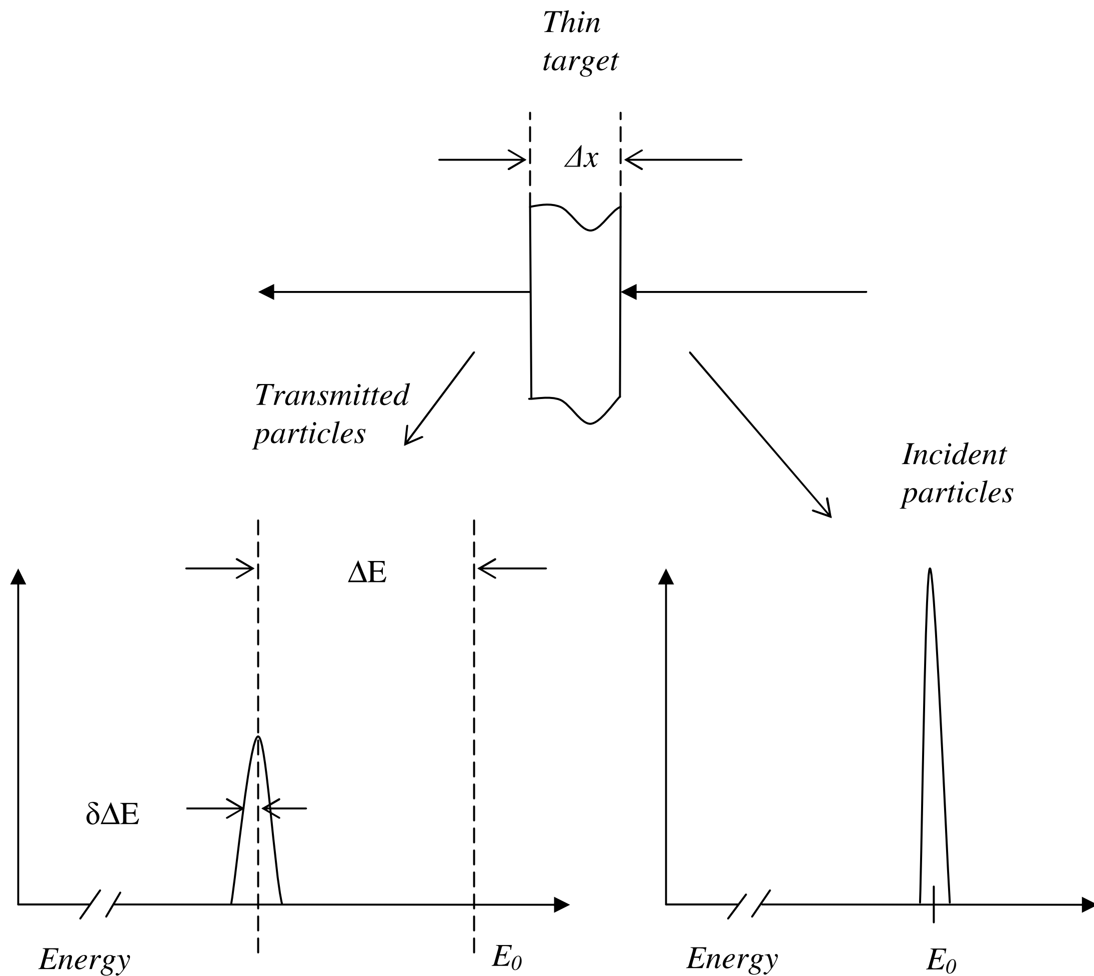

Figure 3-3: A monoenergetic beam of energy E_0 loses energy ΔE in penetrating a thin film of Δx. Simultaneously, energy straggling broadens the energy profile.

In figure 3-3, the ion with initial energy E_0 (sharp peak, right hand side of the figure) is penetrating the target of thickness $t = \Delta x$, resulting in the broadening of the energy peak (left hand side of the figure) after penetration, due to the statistical fluctuations discussed above.

The statistical fluctuations of the nuclear energy loss Q_n^2 are calculated in a similar manner to the nuclear stopping discussed in section 3.1.1, giving [Zie85b]:

$$Q_n^2 = \int_0^\infty T^2 d\sigma = 16\pi Z_1^2 Z_2^2 e^4 \frac{M_1^2}{(M_1+M_2)^2} F_n \qquad \ldots 3.14$$

where: $F_n(\varepsilon) = \dfrac{1}{4 + 0.197\varepsilon^{-1.6991} + 6.584\varepsilon^{-1.0494}}$ and $\varepsilon = \dfrac{M_2 a}{(M_1+M_2)Z_1 Z_2 e^2} E$

From the above equations one can perceive that when E tends to infinity then ε tends to infinity and $F_n = 0.25$. Hence, the maximum of nuclear energy loss tends to:

$$Q_n^2 = 4\pi Z_1^2 Z_2^2 e^4 \frac{M_1^2}{(M_1+M_2)^2} \qquad \ldots 3.15$$

This result means that for high energy projectiles the importance of Q^2_n is negligible (it becomes constant).

The straggling of electronic energy loss is derived from the Bethe – Bloch equation [Boh48]. Using the assumption of a point charge with high velocity, the following equation has been derived [Zie85a]:

$$\Omega_B^2 = 4\pi Z_1^2 Z_2 e^4 N \Delta x \qquad \ldots 3.16$$

where Ω_B^2 is called Bohr straggling. Ω_B^2 is the same as the variance of the average energy loss of a projectile after passing through a target of thickness Δx with Ω_B being the standard deviation. Therefore, the full width at half maximum of energy loss distribution is yielded by $FWHM_B = 2\Omega_B\sqrt{2\ln 2}$. The point charge assumption of Bohr has been extended by Lindhard et al. who included a correction term for energies where the assumptions may not be valid [Lin53].

The total energy straggling in a compound target is found by a linear additivity rule in a similar way to energy loss (Bragg's rule).

3.4 RANGE AND RANGE STRAGGLING

An energetic ion penetrating a material loses energy via nuclear energy loss and electronic energy loss until it comes to rest. Due to the statistical fluctuation of interactions during the energy loss processes, and multiple scattering of the ion from the target atoms, the ion's path zigzags. These statistical fluctuations cause ions with the same energy to be implanted at different depths. The total distance, which the ion travels from the surface to where it stops, is called the total range or just the range and is calculated by taking into consideration the stopping cross sections (see equation 3.3.). The deviation of the range due to energy straggling is called range straggling. Taking all these factors into account, the total range is finally given by: $R_{tot} = \sum l_i$. Where l_i represents the different paths that the ions travel inside the target (see figure 3-4.) Figure 3-4 depicts two charged particles penetrating a material, i.e. one particle with a low incident energy and another with a high incident energy. The ion with the high incident energy evidences almost a straight line path at the beginning due to electronic stopping, while at the end it tends to be a zigzag due to nuclear stopping. For the lower incident energy ion, the path is a zigzag one since the nuclear and electron stopping are of similar magnitudes. The latter takes a shorter path owing to lower energy and many deflections. The projected range R_p is defined as the average penetration depth from the target surface to where the ion comes to rest (measured parallel to the incident direction), while the perpendicular range $R_\perp$ is measured perpendicular to the direction of the incident ion. The total range is always longer than other ranges because it takes into consideration all the ion implanted paths taken inside material.

The gradual increase in the diameter of the ion beam as it passes into a sample, owing to multiple scattering of the ion inside the sample, is known as lateral spread, while the associated increasing distribution in the direction of the ions relative to the initial direction is known as the angular spread. Lateral spread and angular spread can be estimated from multiple scattering theories proposed by Sigmund and Winterbon; Markwick and Sigmund [Sig75] [Mar75]. Angular and lateral spreads also increase the path length and hence energy fluctuations, especially if the path length is not normal to the surface.

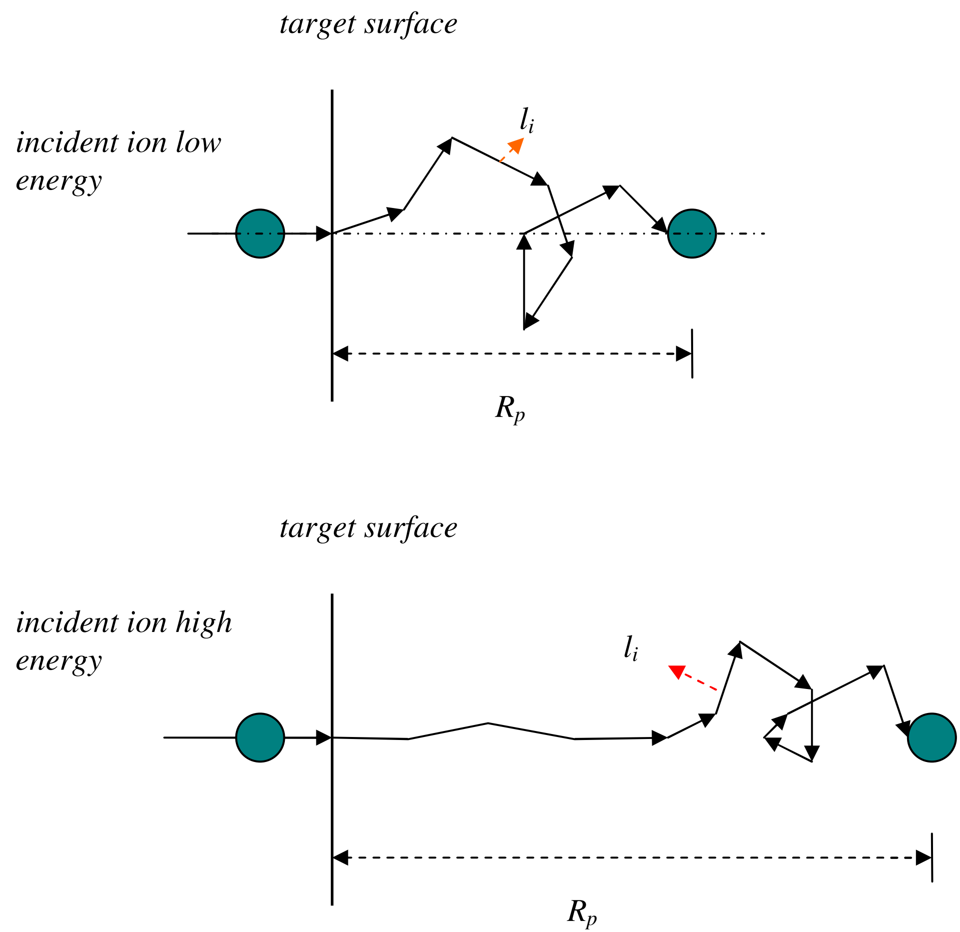

Figure 3-4: Range concepts for incident ions with low (top figure) and high (bottom figure) energies in target material.

The ions with the same initial incident energy have different impact parameters with respect to the atoms; therefore, they will not follow the same path after interacting with the target atoms. This effect varies the number of collisions which the ion undergoes and also the total range. The distribution of the final positions is usually assumed to be Gaussian, as illustrated in figure 3-5. In this figure, the projected range (R_p) is depicted. From range straggling σ the FWHM can be calculated from: FWHM $= 2\sigma\sqrt{2\ln 2}$. Our silver profiles were found to be near Gaussian. The other moments of our distribution are discussed in section 5-6.

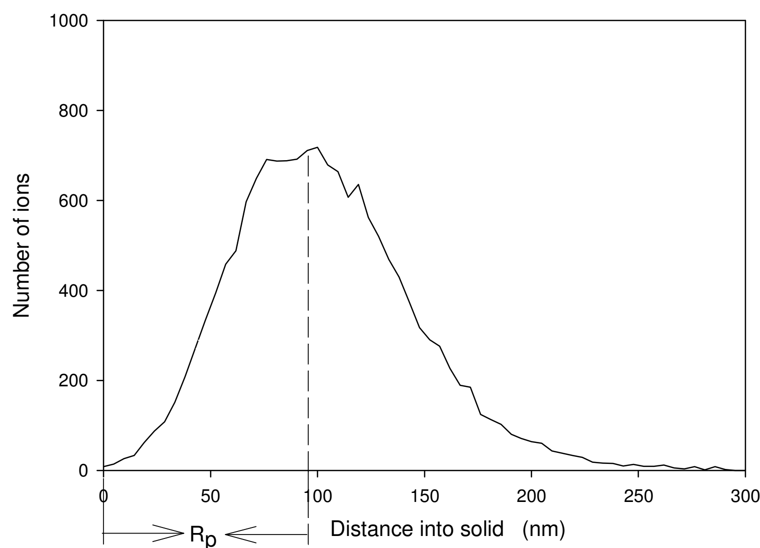

Figure 3-5: The distribution of final implanted ion positions as function of distance in the material.

3.5 ION CHANNELLING

The steering of a beam of energetic ions into open spaces between close-packed rows or planes of atoms in a crystal is called channelling. This channelling effect is illustrated in figure 3-6. The steering is the result of a correlated series of small-angle screened Coulomb scatterings between an ion and atoms bordering the channel. Therefore, channelling occurs in a crystalline solid when an ion beam is well aligned with a low index crystallographic direction. It causes a reduction in the backscattered ions or backscattered yield. This makes channelling very sensitive to crystal disorder and to small displacements of atoms from their crystalline lattice positions. Therefore, at very low fluencies, range distributions for

ions implanted in single crystals differ from those implanted in amorphous targets because of the channelling effect.

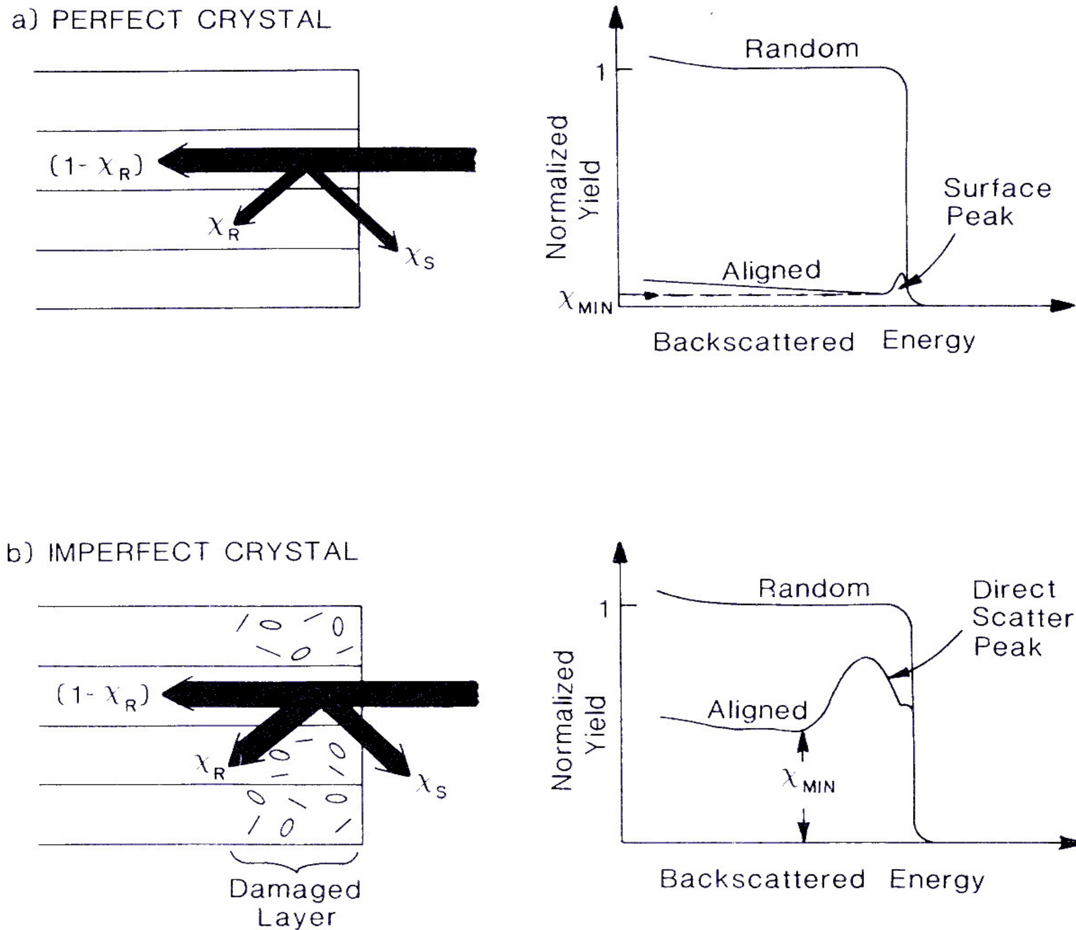

Figure 3-6: Schematic diagram showing ion channelling, dechannelling (χ_R) and direct scattering(χ_S) in a) a perfect crystal, b) an imperfect crystal. The random and aligned spectra are also shown indicating the minimum yield (χ_{MIN}) [Bir89].

For an ion beam entering a crystal parallel to a channel direction, the beam can be separated into a random component χ_R (whose path through the crystal is not affected by regular arrangement) and a channelled component (1-χ_R), which is steered along the open crystal by correlated collisions with the regular arrays of atoms. The backscattered ions χ_S represent a third component which is a very small part of an ion beam during channelling in perfect crystal (see figure 3-6). χ_S contains the information about the identity and distribution of target atoms. During the channelling process some of the channelled ions are scattered away as they penetrate into the solid and are said to be de-channelled. The small peak appearing at the surface in the

aligned RBS spectrum in figure 3-6 is due to scattering from the sample's surface. In an aligned spectrum the surface peak indicates the number of atom layers available for large angle scattering or backscattering, while the normalised yield behind the surface peak corresponds approximately to the minimum random component and is usually termed the minimum yield χ_{MIN}. Since channelling is the result of regular atomic arrangement in crystalline solids; it is sensitive to small disturbances in the crystallinity. Hence the interaction of a channelled beam with crystal defects increases the random components of the beam (by increasing the rate of dechannelling) and the direct small impact parameter collision yield, by introducing lattice atoms into the path of the channelled beam.

The axial channel is defined by rows of atoms around the trajectory i.e. the steering in 2 directions (x,y) perpendicular to the ion velocity (z-direction), while the planar channel is defined by parallel planes; i.e., is the steering of the ion in 1-direction (x) perpendicular to ion velocity (z-direction) [Bir89]. Figure 3-7 depicts the typical channelling spectra from axial and planar alignments. The planar alignment has a high backscattered yield and the spectrum contains distinct yield oscillations in the near surface region. The axial alignment on the other hand has a low minimum backscattered yield while the spectrum has only damped yield oscillation. In perfect or virgin crystals, the typical minimum yield is around 1-5% of random yield for low index axes, whereas low index planes record a minimum yield of around 10-50% of the random yield [Tes95][Gem74][Bir89].

Channelling of ions commencing their trajectories from within the crystals is also possible, namely double alignment and blocking. Double alignment refers to the situation where ions that are initial incident along a channelling direction and scattered ions are detected along the channelling direction. This results in another reduction of backscattered yield and an increase in the sensitivity to lattice disorder and atom location. Blocking denotes the situation where an ion commences its trajectory from a crystal lattice site, which might stem from the spontaneous decay of an unstable lattice atom or from some form of ion beam interaction. This results in minimum backscattering yield when viewed along certain channelling directions,

which might be due to shadowing or blocking by the crystal lattice from outside the crystal.

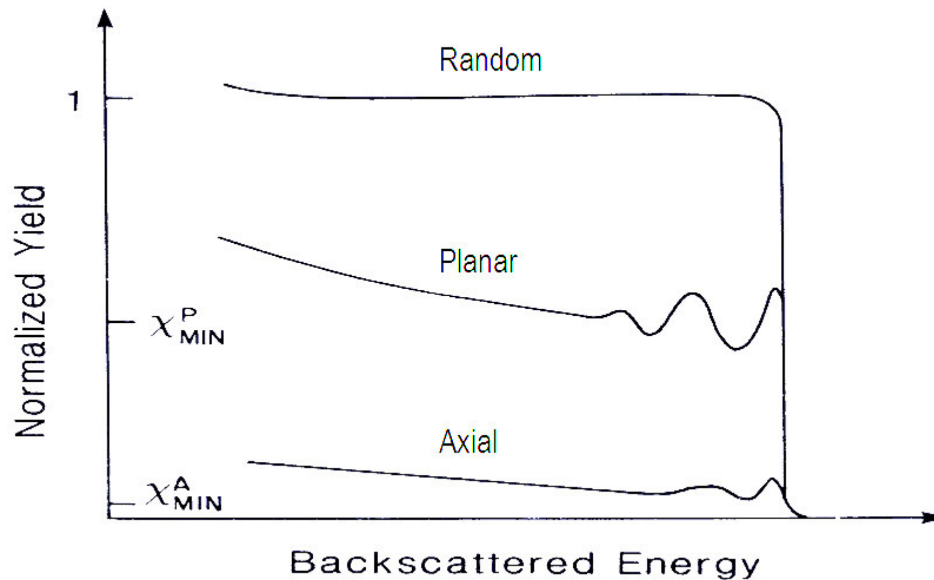

Figure 3-7: RBS-C spectra showing the result of axial and planar channelling [Bir89].

A first order approximation of channelling assumes ion scattering from atomic strings (axial channelling) and planes (planar channelling). These interactions are considered to take the form of a sequence of ion-atom collisions, as illustrated in figure 3-8. This theory is known as the continuum model. This model of channelling states that ion-string or ion-plane scattering can be approximated by scattering from a string or plane of uniform potential, which assumes that the discrete nature of the atoms is insignificant. This is a result of the fact that each steering collision is the average of many individual ion-atom collisions.

Not all the incident ions give rise to the channelling effect discussed above in this section. The channelling effect only occurs if the ion's incident angle is small. Lindhard et al. found that the channelling occurs if the incident angle of ions upon a row of atoms is less than the critical angle ψ_c [Lin65]. This critical angle is yielded by:

$$\psi_c = \left(\frac{2Z_1Z_2e^2}{E_0 d} \right)^{\frac{1}{2}} \qquad \text{....3.17}$$

where d is the atomic spacing along the aligned row and E_0 is the energy of an incident ion. ψ_c is a theoretical parameter that is not directly measured experimentally but is related to the angular half width at half $\psi_{1/2}$ of the angular scans' profiles (see figure 3-9).

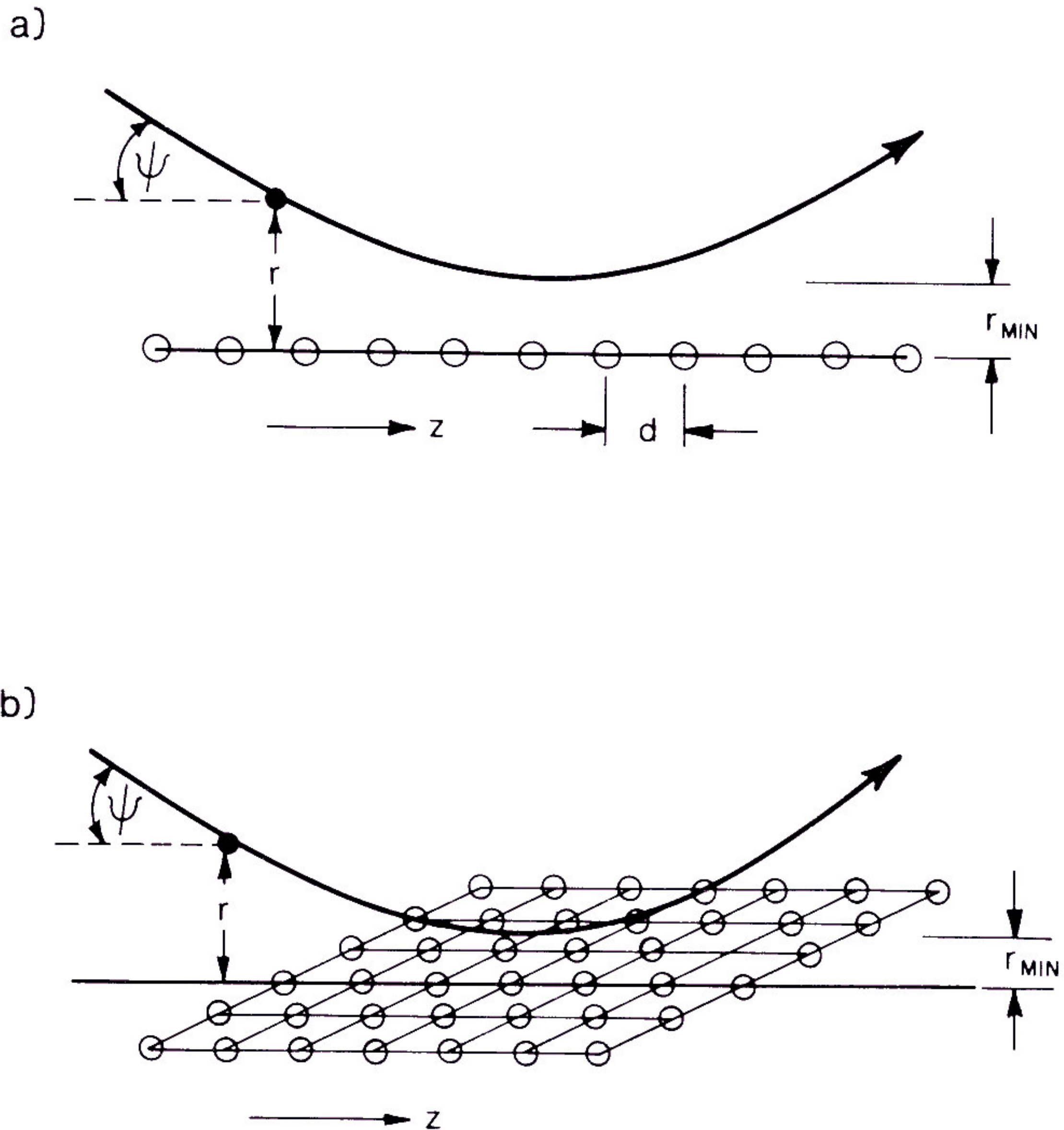

Figure 3-8: Continuum model of channelling from a string only (a) and a plane (b)[Bir89].

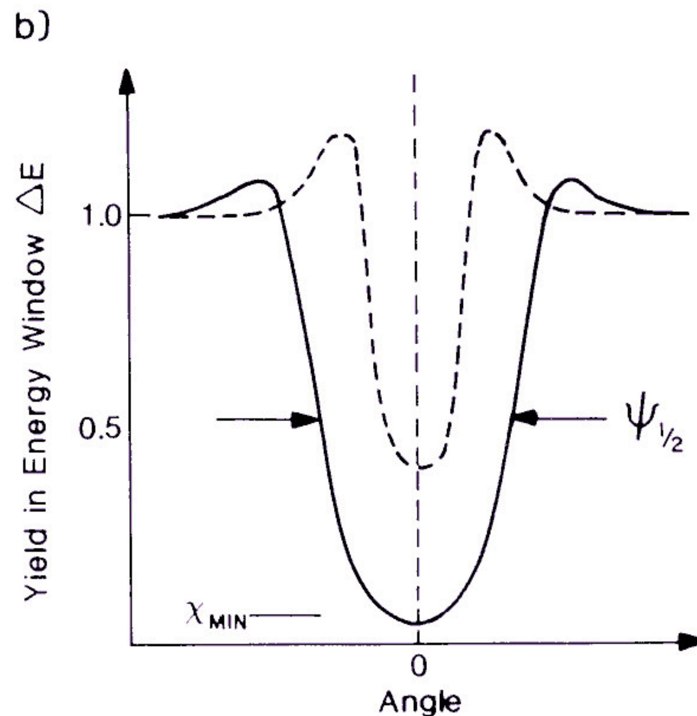

Figure 3-9: The angular yield about an axial channel (solid curve) and a planar channel (dashed curve) indicating the channelling half angle $\psi_{1/2}$ [Bir89].

The discussion of channelling in the section above indicates that channelling is an important technique in analysing the retained damage after the sample is treated, by such a method as implantation in this thesis. In this thesis Rutherford backscattering combined with channelling (RBS-C) was used to study radiation damage retained after silver implantation into 6H-SiC and after annealing. The experimental details of RBS-C are discussed in chapter 4.

3.6 SIMULATION OF ION IMPLANTATION

In order to gain an idea of the ion implantation results before performing the experiment, it is important to start by simulating it. This affords an idea of the expected experimental results. This section discusses the computer simulation performed before the implantation of silver into silicon carbide.

For simulation of ion implantation, radiation damage, sputtering and the reflection and transmission of impinging ions, a computer simulation of slowing down and scattering of ions in materials can be used. In this study the transport of ions in matter (TRIM 98) program was used [Zie85a]. It was developed for determining the ion range, damage range and damage distributions as well as the angular and energy distributions of backscattered and transmitted ions in amorphous targets. Therefore, this program does not take into consideration the channelling of bombarding ions. This program has displays high computing efficiency and maintains a moderate degree of accuracy with approximately 5-10% error. This efficiency is achieved by the fact that TRIM does not take into account the crystal structure or dynamic composition changes in the material that occurs when the ion penetrates materials, since approximations are used in this program. Approximations include the following:

- binary collision (i.e. the influence of neighbouring atoms is neglected);
- recombination of knocked off atoms (interstitials) with the vacancies is neglected;
- the electronic stopping power is an averaging fit from a large number of experiments;
- the interatomic potential as a universal form which is an averaging fit to quantum mechanical calculations;
- the target atom which reaches the surface can leave the surface (be sputtered) if it possesses enough momentum and energy to pass the surface barrier;
- the system is layered, i.e. simulation of materials with composition differences in 2D or 3D is not possible.

During simulation the ion is assumed to change direction as a result of binary nuclear collisions and to move in straight free-paths between collisions. The nuclear and electronic energy losses are considered to be independent, and the ion track is terminated either when the energy drops below a pre-specified value or when the ion position is outside the target in this program. TRIM 98 only works in the ion energy range of approximately 0.1 keV to several MeV, depending on the masses involved [Zie85]. Since nuclear and electronic energy losses are independent, the ions lose energy in discrete amounts in nuclear collisions and continuously in electronic interactions.

The TRIM 98 results of 360 keV silver ions implanted in 6H-SiC, as used in this study, are depicted in figure 3-10 where the simulated silver depth profile is compared with a typical silver depth profile from RBS (the black crossed one). The silver peak from TRIM 98 is almost a Gaussian distribution with the projected range (R_p) =106 *nm*, skewness (γ) = 0.06, kurtosis (β) =2.78 and straggling (σ) = 27 *nm*. The silver profile moments obtained from the typical silver profile measured by RBS are shown at the top of figure 3-10. R_p is in agreement with TRIM predictions but the higher moments are not in agreement with these. TRIM 98 results also indicate that displacement damage starts at the depth of 3 *nm* with the displacement peak situated at about 5 *nm*. The electronic energy loss is higher at the beginning but reduces as it enters deeper into the target, while nuclear energy loss increases. This is due to the fact that as the ion gets deeper into the target, its energy decreases, resulting in increased nuclear energy loss as explained at the beginning of this chapter. The discrepancy between simulation and our RBS results is due to approximations used during TRIM calculations as explained above.

360 keV Ag^+ ⟶ 6H-SiC
T_i=23 °C
F=2x10^{16} cm^{-2}

Rp=109 nm
σ = 39 nm
β = 2.98 nm
γ = 0.15

Relative atomic density (%)

Depth(nm)

Ag^+(360 keV) ⟶ SiC

Total Electronic Energy Loss(eV/nm)

Depth(nm)

Ag^+(360 keV) ⟶ SiC

Total Nuclear Energy Loss(eV/nm)

Depth(nm)

Figure 3-10: Results of Trim 98 calculations for silver (360 keV) implanted on 6H-SiC. A typical silver depth profile (black crosses) measured by RBS is also included on the top figure. The range moments shown in the top figure are obtained from the RBS-measured silver profile.

3.7 REFERENCES

[And77] H.H. Andersen and J.F. Ziegler, Hydrogen Stopping Power and Ranges in all Elements, Vol. 3, Pergamon Press, New York (1977).

[Bet30] H. Bethe, Ann. Phys. (Leipzig) **5** (1930) 324.

[Bic84] H. Bichsel, ICRU Report, **37** (1984)130.

[Bir89] J. R. Bird and J. S. Williams, Ion Beams for Materials Analysis, Academic Press, Australia (1989).

[Blo33] F. Bloch, Ann. Phys. (Leipzig) **16** (1933) 285.

[Boh13] N. Bohr, Phil. Mag., **25** (1913) 10.

[Boh40] N. Bohr, Phys. Rev., **58** (1940) 654.

[Boh41] N. Bohr, Phys. Rev., **59** (1940) 270.

[Boh48] N. Bohr, Matt. Fys. Medd. Dan Vid. Selsk., **24** (1948) 19.

[Bra05] W.H. Bragg and R. Kleeman, Phil. Mag. **10** (1905) 318.

[Car76] G. Carter and W. A. Grant, Ion Implantation of Semiconductor, eds. A. H. W. Beck and J. Lamb, Edward Arnold, London (1976).

[Chu78] W. K. Chu, J. W. Mayer and M. A. Nicolet, Backscattering Spectrometry, Academic Press, New York (1978).

[Gem74] D. S. Gemmell, Rev. Mod. Phys. **46** (1974)129.

[Lin53] J. Lindhard, M. Scharff, K. Dan. Vidensk. Selsk. Mat. Fys. Medd. **33** (1953) No. 15.

[Lin61a] J. Lindhard and M. Scharff, Phys. Rev. **124** (1961) 128.

[Lin61b] J. Lindhard, M. Scharff and K. Dan. Vidensk. Selsk. Mat. Fys. Medd., **33** (1953) No. 14.

[Lin65] J. Lindhard, K. Dan. Vidensk. Selsk, Mat. Fys. Medd. **34** (1965) No. 14.

[Mar75] A. D. Marwick and P. Sigmund, Nucl. Instr. and Meth. **126** (1975) 317.

[Rim95] E. Rimini, Ion Implantation: Basics to Device Fabrication, Kluwer Academic Publisher (1995).

[Sig75] P. Sigmund and K. B. Winterbon, Nucl. Instr.and Meth. **119** (1974) 541.

[Tes95] J. R. Tesmer and M. Nastasi, Handbook of Modern Ion Beam Materials Analysis, MRS, Pittsburgh, USA (1995).

[Tho03] J. J. Thomson, Conduction of Electricity through Gases, Cambridge Univ. Press (1903).

[Zie85a] J. F. Ziegler, and J. M. Manoyan, Nucl. Inst. and Meth. **B35** (1988) 215.

[Zie85b] J. F. Ziegler, J. P. Biersack and Y. Littmark, The Stopping and Range of Ions in Solids, Pergamon Press, (1985).

[Zie88] J.F. Ziegler and Manoyan, J.M. Nucl. Instr. and Meth. **B35** (1988) 215.